University of Groningen

Bachelor Research Project

Design of a Grid-less Retarding Field Analyser for Beams of Multiply Charged Sn Ions

Author:
S. Buitjes *(s4021398)*

Supervisor/Examiner:
prof. dr. ir. R. A. Hoekstra
Daily supervisor:
L.Assink Msc.
Second examiner:
dr. T. A. Schlathölter

June 12, 2023

university of groningen

faculty of science and engineering

Abstract

In order to measure the charge exchange between Sn ions and H_2 gas a Retarding Field Analyser (RFA) is used to distinguish different charge states from each other. Current generation RFA's make use of grids to create a potential barrier for charged particles. However, these grids cause the transmission to become dependent on the retarding voltage. Furthermore, ion collisions with these grids can cause secondary electrons which may affect the measured current. In the research presented here, a new design for a grid-less RFA is presented and tested with the software package SIMION. By increasing the thickness and decreasing the radius of the electrodes, the ratio k between the potential at the center of the electrode $\phi(0,0)$ and the set retarding voltage V_r can be increased to $k \approx 0.99$. Furthermore, by adding an extra ground electrode between the retarding and suppressor electrode and setting the suppressor voltage to $V_s = -100$ V, secondary electrons originating from the Faraday Cup (FC) with $E < 25$ eV will be fully reflected back into the FC. By fitting a Gauss error function to the transmission at the point of full retardation the energy resolution was measured to be 0.27%. However, further simulations need to be done regarding the time of flight of the incoming ions to determine a more accurate energy resolution. It was also shown that the energy distribution of a multiply charged ion beam can be measured with a good accuracy with a grid-less RFA. With this new design for a grid-less RFA no lensing effects were observed near the region of full retardation.

Contents

1 Introduction

Computer chips are one of the most fundamental parts of modern technology. Transistors are getting smaller and smaller to keep up with Moore's law, which states that the computing capacity should double about every 1.5 years. Nowadays, they are made using lithography tools which make use of Extreme Ultra-Violet light (EUV) to print specific patterns on silicon wafers, such as the machines from the Dutch tech giant ASML. The minimum feature size of these patterns depend on the wavelength of the light that is used [1]. Therefore, a very short wavelength of light is needed to create even smaller chips. ASML uses EUV light with a wavelength of 13.5 nm in their next generation nanolithography machines. This very specific wavelength is generated by a Laser Produced Plasma (LPP). Sn droplets are irradiated by a CO_2 laser and the Sn droplets turn in to a plasma which emits light with a wavelength of 13.5 nm [2]. This 13.5 nm light is then focused by use of expensive mirrors to print patterns on a silicon wafer. However, due to the generation of this Sn plasma, Sn ions with a distribution of charges and energy will be emitted and could damage said expensive mirrors. A way to prevent these ions from impacting the mirrors, is to introduce H_2 gas into the system. The Sn ions interact with the H_2 molecules and therefore depleting them of their kinetic energy. During this interaction, also charge exchange between the ions and the gas occurs. However, little is known about the interactions between H_2 molecules and Sn ions and their charge exchange.

The charge exchange between ions and gases such as Sn and H_2, are studied at the ZERNIKE Low Energy Ion-beam Facility (ZERNIKELEIF) of the University of Groningen. The charge composition of ion beams can be measured by use of a Retarding Field Analyser (RFA). In chapter 2 the working principles of an RFA we will be discussed and how lensing affects the transmission of an RFA. In chapter 3 further theoretical information will be given about charge exchange and how changing the geometry of a ring electrode changes its potential field. In chapter 4 the experimental setup at ZERNIKELEIF will be explained briefly, and the software package SIMION will be discussed. Chapter 5 contains the design process of the grid-less RFA, and finally chapter 7 describes the properties of the final design of a grid-less RFA.

2 Retarding Field Analyser

To measure charge composition of an ion beam, a Retarding Field Analyzer (RFA) is used. An RFA is a device that can act as a kind of filter to distinguish charged particles of a certain charge and energy. The RFA used at ZERNIKELEIF is the Kimball Physics FC-73A which is comprised of a Faraday Cup (FC) with four grids in front of it. A picture of this RFA can be seen in figure 1.

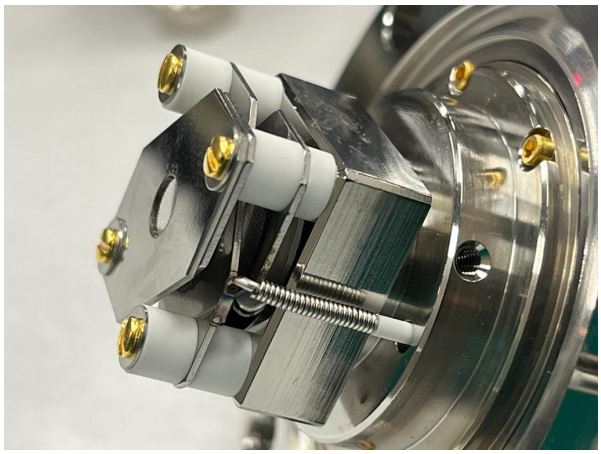

Figure 1: A picture of the grid stack of a disassembled Kimball Physics FC-73A Retarding Field Analyser.

The first grid, is the grounded grid (G) and it is electrically grounded. The second and third grids are the retarding grids (R), which have a retarding voltage V_r applied to them to create a potential barrier. The fourth grid is the suppressor grid (S) and it is negatively biased V_s to reflect secondary electrons coming from the FC back into the FC. The reason grids are used is to make sure a uniform potential is created at the position of the grid. In figure 2 a schematic drawing of this RFA can be seen.

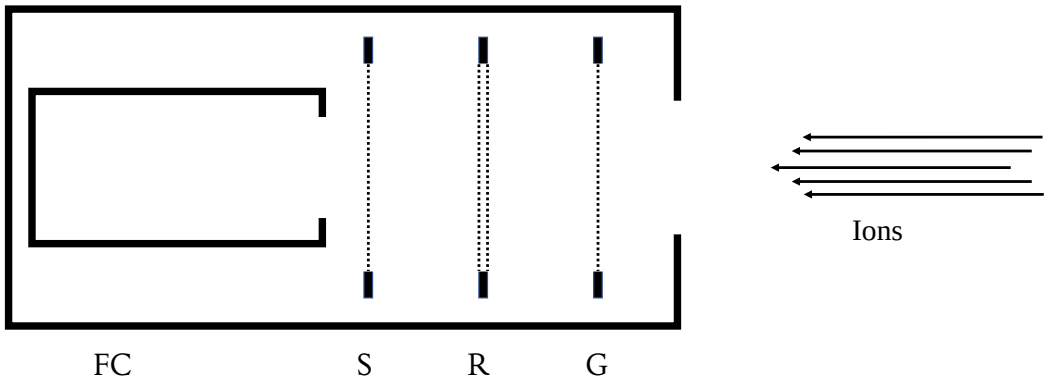

Figure 2: A schematic drawing of ions approaching the RFA with a ground electrode G, a retarding electrode R, a suppressor electrode S, and the Faraday Cup FC.

The retarding voltage set on R generates an electric field between the electrodes and follows Laplace's equation which can be seen in equation 2.1:

$$\mathbf{E} = -\nabla\phi, \tag{2.1}$$

where $\mathbf{E}$ is the electric field of an electrode, and ϕ is the electric potential. This will be used later on to determine ion trajectories. When a charged particle with a kinetic energy E approaches the retarding grid, it will either be reflected away from the retarding grid or it will overcome the potential barrier if its kinetic energy is high enough. The condition for a charged particle to pass the potential barrier is dependent on the following equation:

$$E > qV_r, \tag{2.2}$$

where q is the the charge of the particle in Coulomb. Any charged particle that has a lower kinetic energy than the retarding voltage will be reflected. This process can be seen in figure 3.

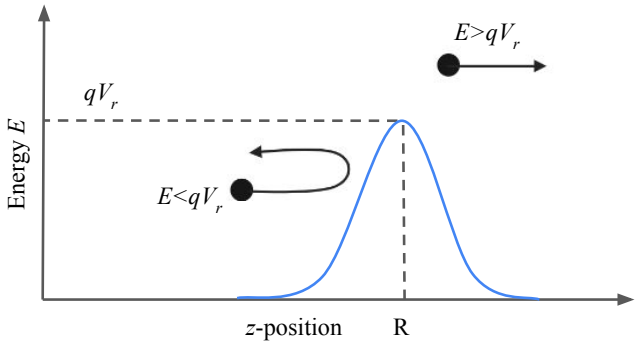

Figure 3: Two ions approaching the potential barrier where one ion has an energy lower than the potential barrier and is therefore reflected, and one ion which has a higher energy than the potential barrier and is therefore transmitted.

2.1 FC Current Measurement

When a charged particle overcomes the potential barrier in the RFA, it can reach the FC. When charged particles reach the FC, their current is measured. This current is proportional to the amount of charged the particles that reach the FC. The current contribution of a particle with a certain charge state can be seen in equation 2.3:

$$I_q = eqN^{q+}, \tag{2.3}$$

where I_q is the measured FC current, q is the charge of a particle in integers, e is the elementary charge given by $e = 1.60217663 \cdot 10^{-16}$ C, and N^{q+} is the number of charged particles measured in the FC per second. Therefore, if a particle beam contains charges

$q = 1+, 2+, 3+$ and no bias voltage is applied, then the measured current is equal to the charges' individual contributions as seen in equation 2.4.

$$I_{tot} = (3N^{3+} + 2N^{2+} + 1N^{+})e \tag{2.4}$$

The individual contributions of the charged particles can be measured by setting the retarding voltage such that only those of a certain charge state will be transmitted. For a kinetic energy of $E = 4000$ eV, the FC current for an ion beam with charges $q = 1+, 2+, 3+$ can be seen in figure 4. However, to determine the contribution of the

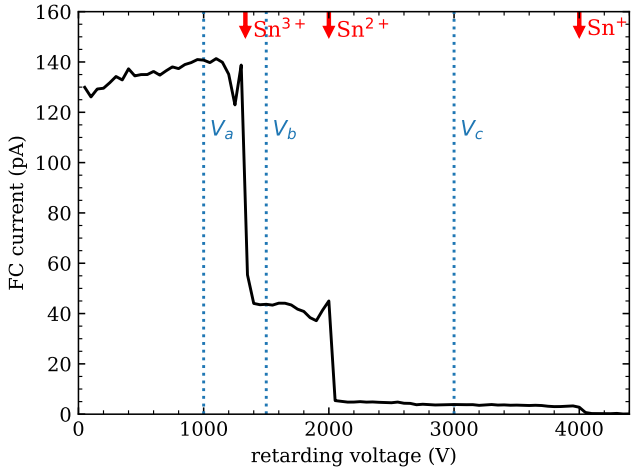

Figure 4: The FC current of a multiply charged 4 keV ion beam with removed background currents.

3+ Sn ions in figure 4 and following equation 2.4, the contributions of the 2+ and 1+ particles first need to be determined. When the current is measured at a voltage V_c, only the current contribution of $q = 1+$ particles will be measured such that

$$I_1 = I(V_c). \tag{2.5}$$

Then, by setting the retarding voltage to V_b the current contribution of $q = 2+$ particles can be calculated by

$$I_2 = I(V_b) - I_1. \tag{2.6}$$

In turn, the current contribution of $q = 3+$ particles can be calculated by

$$I_3 = I(V_a) - I_2 - I_1. \tag{2.7}$$

By using equation 2.3, the amount of particles for each charge state that reach the FC can be calculated such that the total amount of particles that reach the FC is equal to

$$N_0 = N_3 + N_2 + N_1 = \left(\frac{I_3}{3} + \frac{I_2}{2} + \frac{I_1}{1}\right)\frac{1}{e}. \tag{2.8}$$

Therefore, the amount of particles of a certain charge state compared to the total amount of particles that reached the FC can be determined by the ratio of the two.

$$\frac{N_q}{N_0} = \frac{I_q/q}{\frac{I_3}{3} + \frac{I_2}{2} + \frac{I_1}{1}} \tag{2.9}$$

2.2 Suppressor Grid

When an ion reaches the FC, a current is measured. But during the collision with the FC, secondary electrons can be emitted which can end up outside of the FC. When this happens, a change in current will be measured which would result in false measurements. To prevent such false measurements, a suppressor grid is placed in front of the FC, see figure 2, at a negative bias voltage to reflect electrons back into the FC. A schematic drawing of an electron being reflected back into the FC can be seen in figure 5.

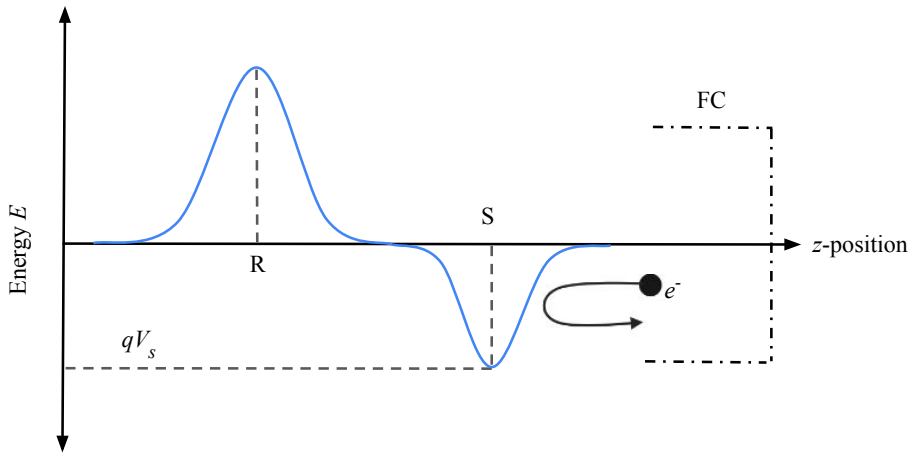

Figure 5: An electron being reflected back into the FC by a negatively biased suppressor grid.

2.3 Grounded Grid

Next to the retarding and suppressor grids, there is also a grounded grid placed in front of the retarding grid. As the name implies, this grid is electrically grounded. If this grid was not there, the electric field of the retarding grid could extend to outside of the diaphragm of the RFA. This electric field can cause a lensing effect before the charged particles even enter the RFA. Due to the placement of the grounded grid, the electric field lines do not extend to the diaphragm of the RFA.

2.4 Grid Effects on the Transmission

If a ring electrode is biased with a voltage, the potential in the ring will be lower than the potential on the electrode itself with its center being the minimum. If such an electrode was used as a potential barrier for charged particles the bias voltage on the electrode should be higher such that the minimum potential the condition in equation 2.2. However, this makes the bias voltage at which a charged particle gets reflected dependent on the radial position of the particle. In an ion beam, the ions can have a variety of radial positions, which causes the FC current to decrease when the bias voltage is increased until the minimum potential satisfies equation 2.2. However, in a multiply charged ion beam this will happen for all charge states, which means that the current contribution of a certain charge state will already decrease even though other charge states are still able to reach the FC. This means that the transmission curves for different charge states overlap and they cannot be distinguished from each other.

The interwoven wires that form a grid solve this problem because they have the same bias voltage applied to them as the electrode. However, even though this solves the problem of overlapping transmission curves, they give rise to some other effects. Ions can collide with the grids and those collisions can generate secondary electrons which can influence the measured FC current. When ions collide with the grounded or retarding grids these secondary electrons can still be reflected by the suppressor grid. If the ions collide with the suppressor grid, there is no potential barrier stopping these secondary electrons from reaching the FC and influencing the FC current. The grids cause the transmission of an RFA to be dependent on the retarding voltage before an ion beam is entirely reflected [3]. When the retarding voltage approaches the point of full retardation, the potential field around the grid prevents the ions from colliding with the retarding grids and are focused on the suppressor grid [4] which causes the FC current to decrease before it increases again since the ions will not be focused on the suppressor grid anymore. A schematic drawing of such an FC current can be seen in figure 6.

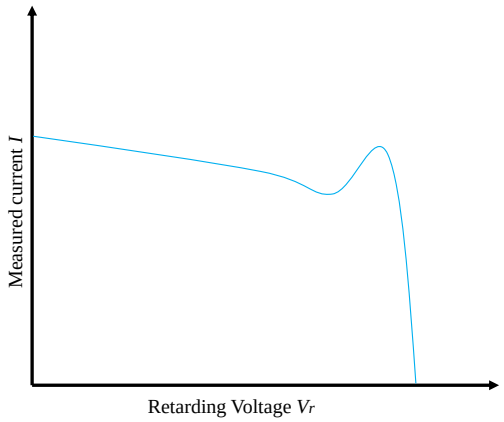

Figure 6: A schematic drawing of the measured FC current where the decrease in current caused by the lensing effect that focuses the ions on the suppressor grid can be seen before full retardation.

Grid misalignments also strongly influence the transmission of a four gridded RFA, and since the specification of the grid alignment is not provided with RFA's such as the Kimball Physics FC-73A, the resulting transmission curves can vary per RFA. Therefore, the possibility of a grid-less RFA is researched such that the charge composition of a monoenergetic ion beam can be accurately determined.

3 Theory

3.1 Sn Collisions with Hydrogen

When Sn ions interact with hydrogen gas, they can transition into a different charge state. In equations 3.1 and 3.2 examples of such reactions can be seen.

$$Sn^{3+} + H_2 \rightarrow Sn^{2+} + H_2^+ \tag{3.1}$$

$$Sn^{3+} + H_2 \rightarrow Sn^{+} + 2H^+ \tag{3.2}$$

To analyse how likely each interaction occurs, Sn ions are traversed through hydrogen gas where they can interact and reactions such as equations 3.1 and 3.2 can occur. The ions that exit the gas cloud will be detected in the FC where a current is measured that is proportional to the number of charged particles that reach the FC. By increasing the pressure of the collision chamber, the probability of Sn ions undergoing charge exchange increases as it is more likely for them to interact with the hydrogen gas. Because Sn^{3+} undergoes charge exchange, the current in the FC decreases. Using this principle, the amount of charge exchange can be determined [5]. By adding grids in front of the FC to create an RFA, the charge exchange can be determined without varying the pressure in the collision chamber. This makes measuring charge exchange a lot easier. In the next section, the geometric properties of a grid-less RFA will be discussed.

3.2 Grid-less RFA

In chapter 2, the principles of an RFA were discussed and how it can be used to measure charge exhange. However, a four gridded RFA is not the most ideal way to measure charge exchange as the transmission depends on the retarding voltage due to lensing effects that are caused by the grids. Furthermore, secondary electrons are generated due to ions colliding with the grids. Therefore, a better way to measure charge exchange would be an RFA that does not make use of grids. This might come with some other issues, as the grids were used to generate a uniform potential in the ring electrode. In 1985 Sakai et al. [6] analytically described how the potential at the center of a ring electrode depends on the thickness of the electrode, the distance between the wires, and on the applied voltage to the grid. This description focuses on three electrodes with the center one being the retarding electrode with a voltage V_r, and the two outer ones being grounded. The retarding electrode has a thickness d and a hole in its center with radius R. The electrodes are a distance l apart from center to center. An illustration of these electrodes can be seen in figure 7.

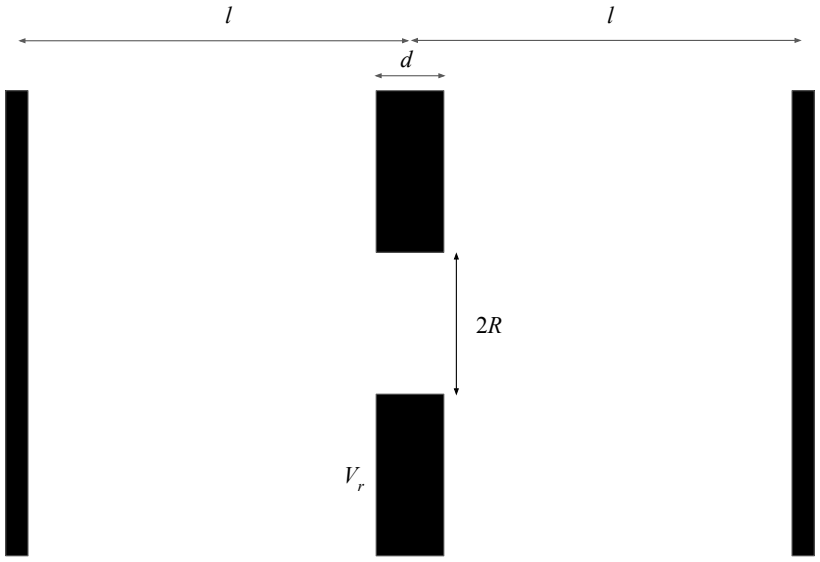

Figure 7: Three electrodes with the center electrode being the retarding electrode with a hole.

Let $\phi(r, z, V_r)$ be the potential as a function of the radial position r, axial position z, and the retarding voltage V_r. According to Sakai, the relation between the potential at the center of the hole and the retarding voltage is dependent on R, d, and l. This relation is given by:

$$\phi(0,0,V_r) = \left\{1 - \frac{R}{\pi l}\left[1 + \frac{d}{R}\tan^{-1}\left(\frac{d}{2R}\right) - \frac{d}{R}\tan^{-1}\left(\frac{d}{R}\right)\right]\right\} V_r. \tag{3.3}$$

Let k be defined as:

$$k = \left\{1 - \frac{R}{\pi l}\left[1 + \frac{d}{R}\tan^{-1}\left(\frac{d}{2R}\right) - \frac{d}{R}\tan^{-1}\left(\frac{d}{R}\right)\right]\right\}. \tag{3.4}$$

Such that,

$$\phi(0,0,V_r) = kV_r. \tag{3.5}$$

The scenario described above can be interpreted as a basic version of a grid-less RFA. So to improve the functionality of this grid-less RFA to work as intended, the geometry of the electrodes should be tuned such that $k \to 1$. Since $\lim_{x\to\infty} \tan^{-1}(x) = \frac{\pi}{2}$:

$$\begin{aligned}\lim_{d\to\infty} k &= \left\{1 - \frac{R}{\pi l}\left[1 + \lim_{d\to\infty}\frac{d}{R}\left(\lim_{d\to\infty}\tan^{-1}\left(\frac{d}{2R}\right) - \lim_{d\to\infty}\tan^{-1}\left(\frac{d}{R}\right)\right)\right]\right\} \\ &= \left\{1 - \frac{R}{\pi l}\left[1 + \lim_{d\to\infty}\frac{d}{R}\left(\frac{\pi}{2} - \frac{\pi}{2}\right)\right]\right\} = \left\{1 - \frac{R}{\pi l}(1+0)\right\} = 1 - \frac{R}{\pi l}.\end{aligned}$$

As can be seen in figure 7, l also depends on d such that $l \to \infty$ as $d \to \infty$. Therefore,

$$\lim_{d\to\infty} k = 1 - \lim_{l\to\infty}\frac{R}{\pi l} = 1 - 0 = 1.$$

This behaviour can also be seen in figure 8a. For the situation where $R \to \infty$, $\lim_{R\to 0}(d/R) = \infty$ such that $\lim_{x\to\infty} \tan^{-1}(x) = \frac{\pi}{2}$ and therefore:

$$\begin{aligned}\lim_{R\to 0} k &= \left\{1 - \lim_{R\to 0} \frac{R}{\pi l}\left[1 + \lim_{d/R\to\infty} \frac{d}{R}\left(\lim_{d/R\to\infty} \tan^{-1}\left(\frac{d}{2R}\right) - \lim_{d/R\to\infty} \tan^{-1}\left(\frac{d}{R}\right)\right)\right]\right\} \\ &= \left\{1 - \lim_{R\to 0} \frac{R}{\pi l}\left[1 + \lim_{d/R\to\infty} \frac{d}{R}\left(\frac{\pi}{2} - \frac{\pi}{2}\right)\right]\right\} = \left\{1 - \lim_{R\to 0} \frac{R}{\pi l}(1+0)\right\} \\ &= 1 - \lim_{R\to 0} \frac{R}{\pi l} = 1 - 0 = 1.\end{aligned}$$

This is shown in figure 8b. Of course when $R = 0$ then it is just an electrode without a hole. Therefore, by making the hole in the retarding electrode smaller and the thickness of the electrode longer, the value of k approaches 1 which means that the potential at the center of the electrode is almost equal to the retarding voltage set on the electrode. This was shown in earlier work by Hwang in 2020 [7].

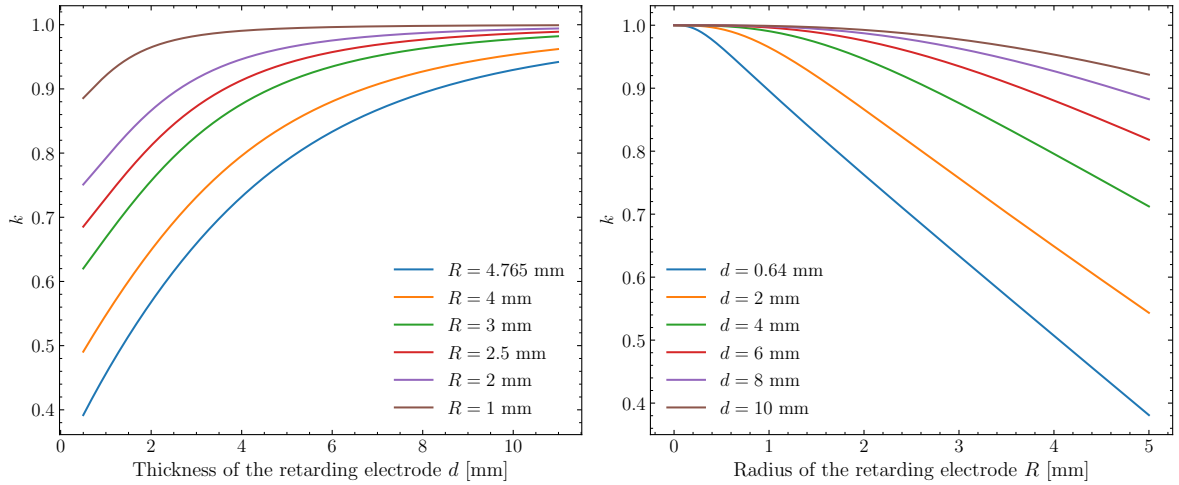

(a) (b)

Figure 8: Equation 3.4 plotted against the thickness of the electrode d for various radii (figure 8a) and the radius of the hole in the electrode R for various thicknesses (figure 8b).

4 Experimental Setup

The experiments carried out by the Ion Interactions group to investigate the charge exchange between Sn ions and hydrogen gas are performed at the ZERNIKE Low Energy Ion-beam Facility (ZERNIKELEIF). In figure 9 a schematic drawing can be seen of the part of ZERNIKELEIF that is relevant for this study. In the ion source, a plasma of

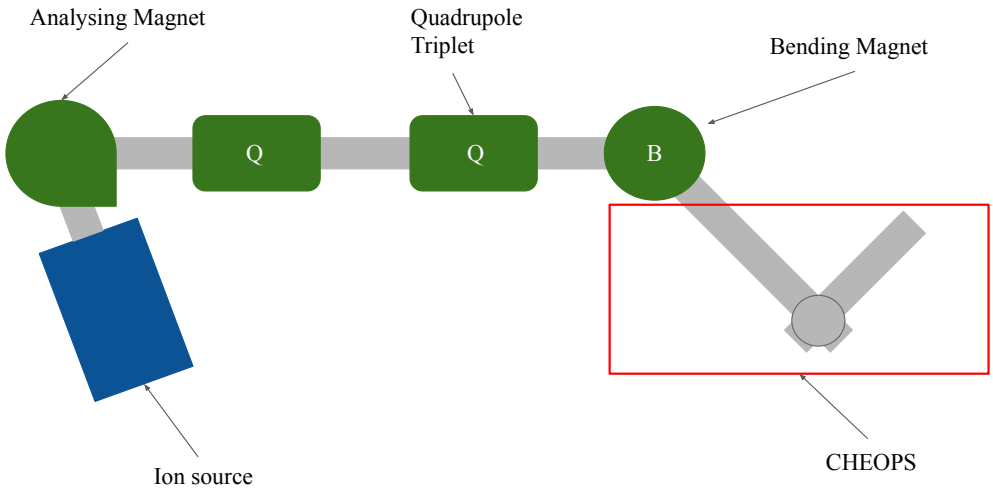

Figure 9: The experimental setup used at ZERNIKELEIF.

the element in question is created from which ions are extracted towards the Analysing Magnet. Since the magnetic field needed to bend a charged particle depends on $B \propto m/q$, the magnetic field strength can be tuned such that only the particles with a specific mass and charge will be directed towards the first quadrupole triplet. The ion beam is then focused by two quadrupole triplets and then travels to the bending magnet where it will be redirected by 45° towards the CHEOPS setup marked with the red outlining in figure 9.

4.1 CHEOPS

Charge Exchange Observed by Particle Spectroscopy (CHEOPS) is the experimental setup used at ZERNIKELEIF to study ion-gas interactions. In figure 10 a schematic drawing of CHEOPS can be seen. The ion beam enters the system on the left and travels through hydrogen gas and eventually arrives at the RFA.

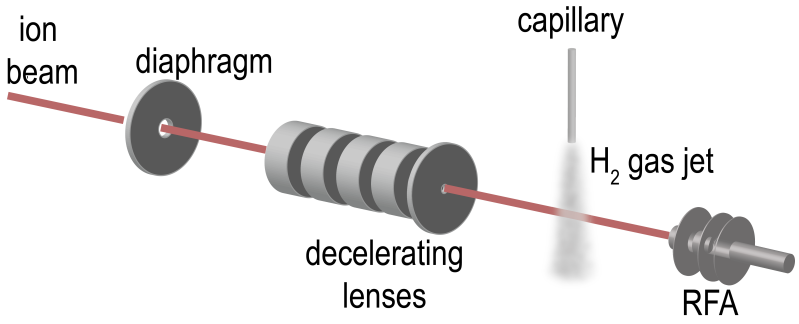

Figure 10: A schematic drawing of the CHEOPS setup.

4.2 SIMION

The software package used to perform simulations of a grid-less RFA is called SIMION. SIMION is a simulation software which can simulate the trajectories of charged particles through electric fields. It does this by discretizing each point in space by a so called grid point. Geometries can be defined using grid points and can consist of separate electrodes which can be biased individually. An electrode is a collection of grid points which together form a potential array (PA). If there are unassigned grid points, SIMION recognizes this as empty space. For the entire geometry, Laplace's equation, as can be seen in equation 2.1, needs to be solved for the entire volume at each grid point. For each grid point, 10 bytes of RAM is needed to compute the potential at that point. Therefore, the discretization needs to be chosen with caution such that the simulation can be done with a realistic amount of memory.

For SIMION to recognise something as a solid, it needs to be at least 2 grid units (gu). Therefore, the resolution needs to be chosen such that the smallest possible length is at least 2 gu. The smallest possible length in the geometry used for the simulations done in this thesis is $L_{min} = 0.64$ mm. Therefore, the minimum resolution R needed is $R = 0.32$ mm/gu. Ideally, all the dimensions of the geometry should be divisible by the resolution and thus, a resolution of $R = 0.01$ mm/gu would be perfect. However, the computing power should also be considered. Since the largest dimension of the geometry is around $L_{max} \approx 38$ mm, the number of grid points needed for this simulation is $(38/0.01)^3 = 3800^3 = 5.4873 \cdot 10^{10}$ grid points. Since SIMION uses 10 bytes of RAM per grid point, this model would take up around 0.5 Tera byte of RAM. Therefore, a lower resolution of $R = 0.1$ mm/gu is chosen such that the amount of memory needed is around $(38/0.1)^3 \cdot 10$ bytes ≈ 500 Mb, which is an acceptable amount of memory.

5 Design Optimisation of a Grid-less RFA

In the following section, the design process towards a grid-less RFA is described. As mentioned in the previous section, the software package used for these simulations is SIMION. As a first step, the current RFA design without the grids is simulated. In figure 11a the geometry of the current RFA design without grids can be seen, and in figure 11b the potential landscape of this design illustrated.

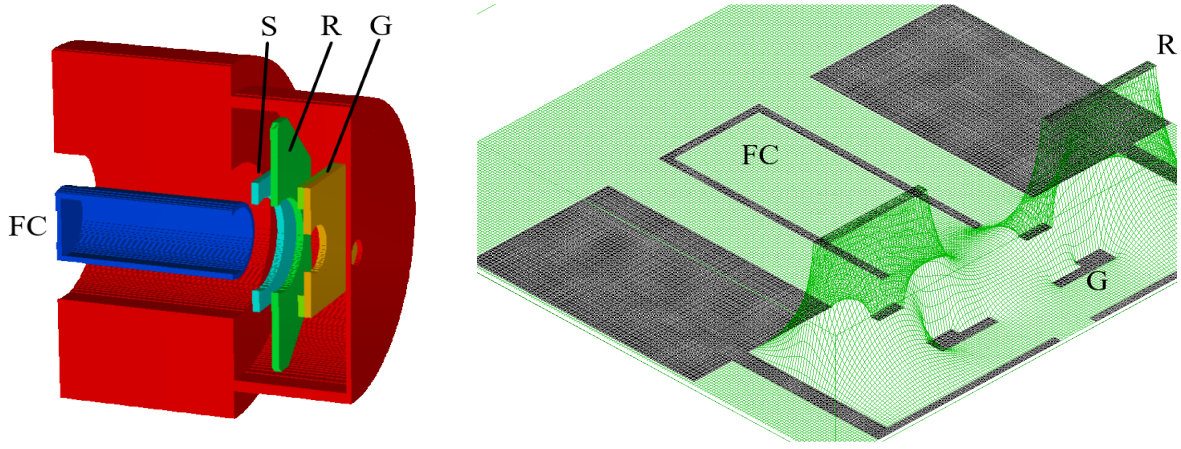

(a) (b)

Figure 11: Current RFA model without grids (11a) and its potential landscape (11b) with V_r=3000 V and V_s=-100 V. In figure 11a the FC is displayed by the color blue, the suppressor electrode in light blue, the retarding electrode in green, and the grounded electrode in yellow.

From the potential landscape in figure 11b it can be seen that in the center of the retarding electrode, the potential is a lot lower than the retarding voltage set on the electrode. The goal is to adjust the design of the RFA such that this sagging effect can be reduced. The potential at the center of the electrode is described by equation 3.5. In figure 12a, the transmission of various energies has been plotted for Sn^{3+}. To determine k of this system, the potential at the center of the electrode needs to be divided by the retarding voltage. The retarding voltage at which an ion beam is fully reflected such that $N/N_0 = 0$ means that $\phi(0,0) = E/q$. Therefore, from the retardation voltages of the transmissions that can be seen in figure 12a, k can be determined by making a linear fit between $\phi(0,0)$ and the retardation voltages.

By performing a linear fit as can be seen in figure 12b, the value of k for this system was determined to be $k \approx 0.21$. This value is quite low as the ideal value of k should approach 1. In figure 12a can be seen that the transmissions of different energies drop long before they are fully reflected. This causes the transmissions of different energies or charge states to overlap with each other, making it harder to distinguish them from each other.

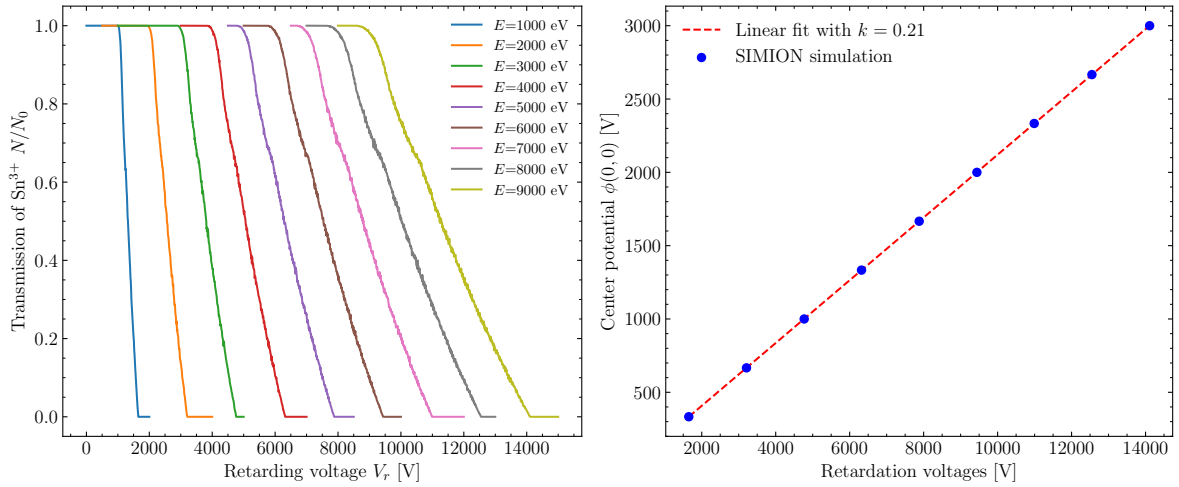

(a) (b)

Figure 12: The transmission of monoenergetic Sn^{3+} beams for various energies (figure 12a) and the potential at the center of the retarding electrode plotted versus the retardation voltages with a linear fit that gives $k = 0.21$ (figure 12b).

In figure 13 the transmission of a multiply charged monoenergetic Sn beam can be seen. From this plot one can see that higher charge states are more difficult to distinguish from each other as the transmission of lower charge states already starts to decrease before the higher charge state is fully deflected.

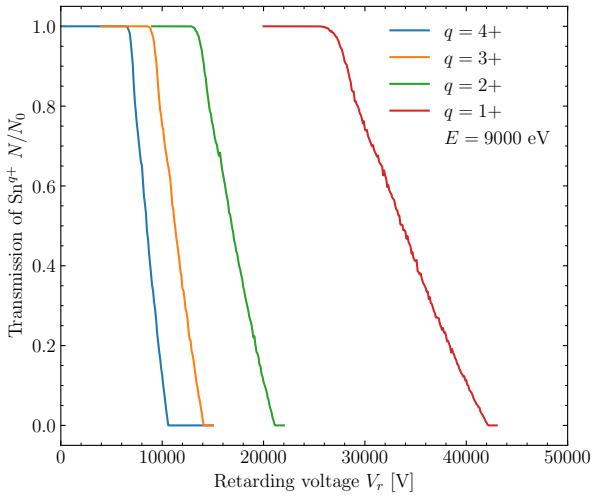

Figure 13: The transmission of a multiply charged and monoenergetic Sn beam with $E = 9000$ eV.

The reason the transmissions have a decreasing slope way before they are fully reflected is because the potential in the electrode varies radially with $\phi(0,0) = kV_r$ and $\phi(R,0) = V_r$ where R is the inner radius of a ring electrode. Therefore, charged particles traveling at a radius r with $R > r > 0$ will be reflected earlier than charged particles traveling

at $r = 0$ since $\phi(r, 0) > \phi(0, 0)$. If the geometry is adjusted such that $k \to 1$, the radial dependence of the potential decreases and such, the slopes of the transmissions will also be steeper and different charge states and energies can be more easily distinguished from each other. In figure 14 a schematic drawing of a ring electrode is shown. Without changing the geometry of the RFA, the slope of the transmission can also be made steeper by having a more focused beam. As mentioned before, this is because the potential in the hole is radially dependent.

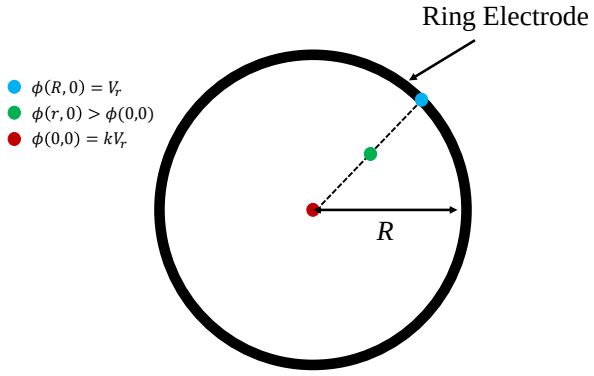

Figure 14: A schematic drawing of a ring electrode with an inner radius R. The red point in the drawing represents the minimum potential in the ring electrode which is given by equation 3.5. The blue point represents the retarding potential V_r set on the electrode. The green point represents the potential at a radius r where $0 < r < R$ and $\phi(0,0) < \phi(r,0) < \phi(R,0)$.

At ZERNIKELEIF, not only Sn interactions with H_2 gas is studied, but also lighter elements like He. To check whether or not the mass of the ions in the ion beam influences the transmission, the transmission for Sn^{3+} ($m = 118.71$ u) and He^{3+} ($m = 4.002$ u) have been plotted with $E = 5000$ eV. In figure 15 can be seen that the transmission perfectly overlaps for both masses. Therefore, the mass does not influence the slope of the transmission. The retardation voltage of an ion beam does not depend on the mass, since it only depends on the ions energy and charge state according to equation 2.2.

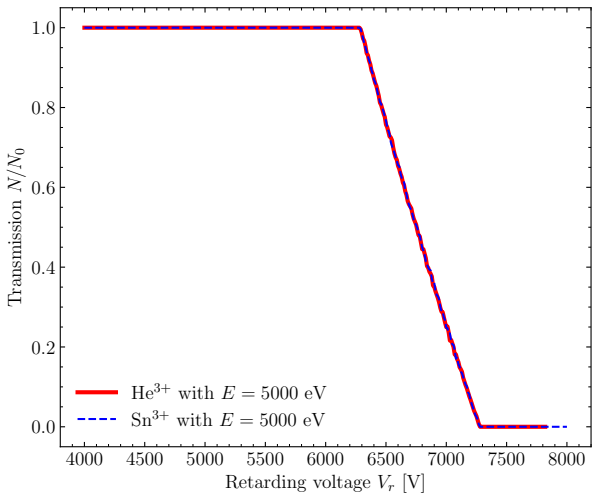

Figure 15: Transmission of Sn^{3+} and He^{3+} with $E = 5000$ eV.

5.1 Geometric Effects on Transmission

Since the value of k of an RFA with only its grids removed is only $k \approx 0.21$, its design needs to be adjusted to improve this value. Some of the geometric features that can be varied to see the effect on k are the inner radiusof the retarding electrode, the thickness of the retarding electrode, and the relative position of the retarding electrode w.r.t. the suppressor electrode and grounded electrode.

5.1.1 Radius of the Retarding Electrode

As described by equation 3.4 and figure 8b, the inner radius of the ring electrode can have a very large influence on the value of k. To see how the radius of the retarding electrode influences k in a grid-less RFA and how it compares to the analytical model described by Sakai, only the radius of the retarding electrode is varied while having a constant thickness of $d = 0.64$ mm and a constant distance between the plates $l = 1.55$ mm. The value of k is determined by dividing the minimum potential $\phi(0,0)$ by the retarding voltage V_r set on the electrode. In figure 16 it can be seen how the values determined

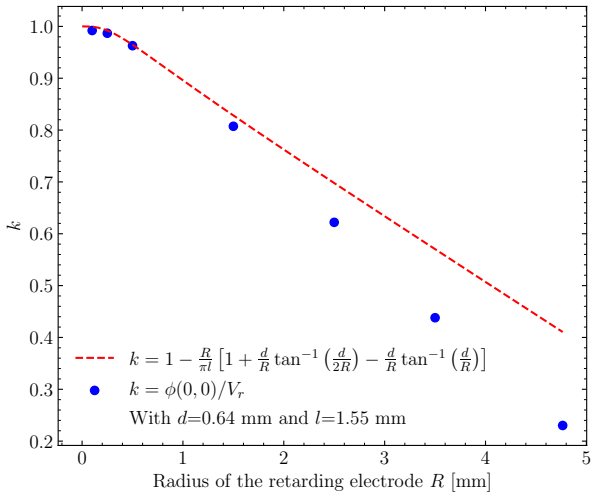

Figure 16: The value of k determined from the SIMION simulations as a function of the radius of the retarding electrode R in mm.

using SIMION approach the theoretical values of equation 3.4 when $R/d < 1$. In this regime the effect of the suppressor and ground electrodes can be neglected and they can be assumed to be grounded electrodes without a hole like in the model presented by Sakai. However, when selecting a radius for the retarding electrode, the radius of the diaphragm and ion beam must also be taken into account. The typical beam width of a generated ion beam at ZERNIKELEIF is around $d = 1.5$ mm [8]. The diaphragm needs to have a larger radius than the ion beam such that minimal collisions occur on the cap of the RFA. The same holds for the electrodes within the RFA. Therefore, the radii of the electrodes are limited by the radius of the diaphragm. If the radius of the retarding electrode is equal to the radius of the ion beam, it is more likely for the ions to interact physically with the electrode. Therefore, a radius needs to be chosen such

that there is a margin between the ion beam and the electrodes while still having a k value that is accurate enough. In figure 17 the geometry and potential lines in SIMION can be seen for $R = 4.765$ mm and $R = 1.5$ mm at $V_r = 500$ V and $V_s = -100$ V.

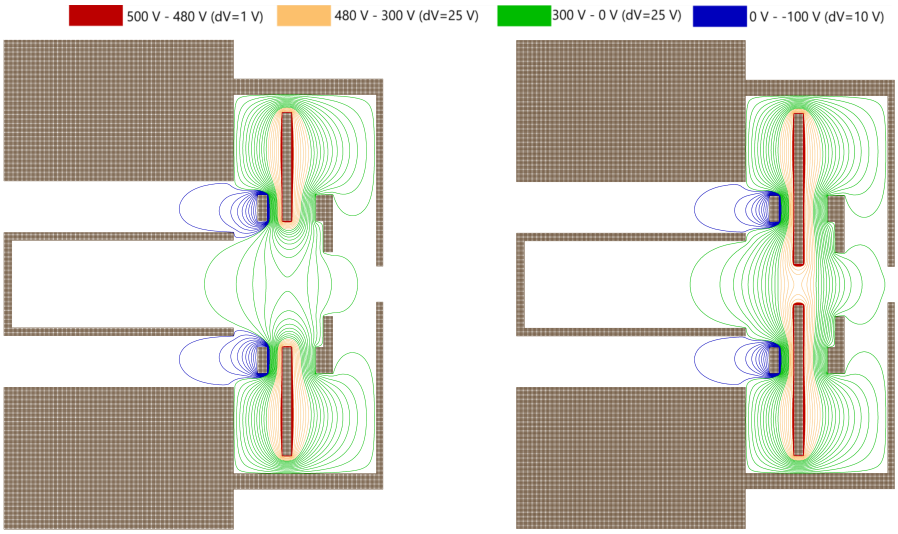

Figure 17: SIMION simulation of a grid-less RFA with $R = 4.765$ mm (left) and $R = 1.5$ mm (right). In the legend above it can be seen that different values of dV are used for different colors. In the red region (500 V-480 V), the distance between two potential lines is 1 V. However, in the yellow and green regions $dV = 25$ V. From this can be seen that the potential rapidly decreases close to the electrode.

In this figure can be seen that the red lines in both scenarios are only around the retarding electrode. However, for $R = 1.5$ mm the yellow potential lines extend to the center of the retarding electrode. This means that the potential in the center is higher for $R = 1.5$ mm than for $R = 4.765$ mm.

5.1.2 Thickness of the Retarding Electrode

The dependence of k on the thickness of the electrode d was also described in equation 3.4 and figure 8a. As mentioned in chapter 3.2, the value of k shall approach 1 as $d \to \infty$. To investigate if this is also the case for a grid-less RFA, d is varied in thickness while keeping R and the distance between the electrodes (excluding the thickness of the retarding electrode) constant. The thickness was varied in steps of the original thickness of the plate from $d = d_0$ to $d = 15d_0$ where $d_0 = 0.64$ mm. In figure 18, the SIMION simulations are shown for $d = d_0$ and $d = 15d_0$ along with their respective potential lines.

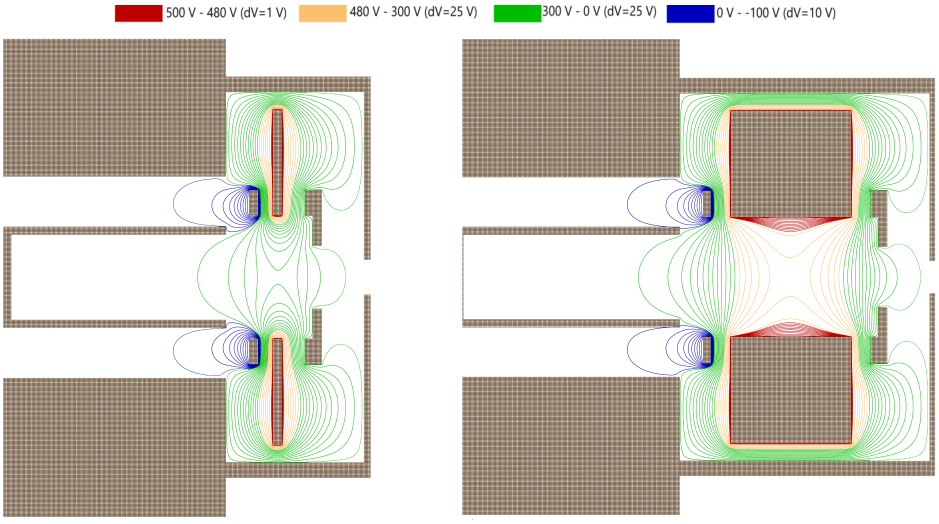

Figure 18: SIMION simulations of a grid-less RFA with $d = d_0$ (left) and $d = 15d_0$ (right) with their potential lines. The colors displayed here have the same properties as in figure 17.

Figure 19 shows the result of these simulations, and it can be seen that the increase in k follows the theoretical behaviour from equation 3.4 but shifted downwards. This downwards shift can be explained by the fact that the system described by Sakai does not have the same geometry as the geometry described here. Sakai assumes three electrodes where only the center electrode has a small hole. In the case of a grid-less RFA, all three electrodes have a hole in them. Even though the geometries of both models are different, k still increases when d increases in the same way as equation 3.4. Figure 19 shows that even with a large radius ($R = 4.765$ mm) the value of k can increase to $k = 0.9$ if the thickness of the electrode is around $d = 10$ mm.

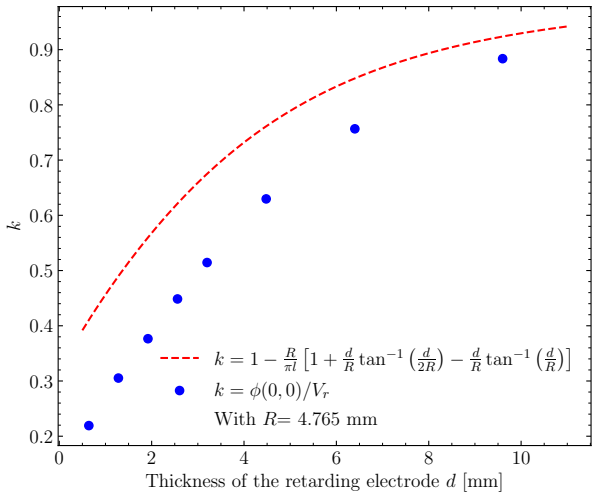

Figure 19: The value k plotted as a function of the thickness of the retarding electrode d in mm together with the SIMION results for k where $R = 4.765$ mm.

5.1.3 Position of the Retarding Electrode

To determine how the position of the retarding electrode influences the transmission, equation 3.5 can be used to plot k versus the position of the retarding electrode. By dividing $\phi(0,0)$ with a constant value of V_r, k can be determined for each z. The distance between the suppressor electrode and grounded electrode is fixed at 3.81 mm, and the position of the retarding electrode is varied in between this region. At a position of $z = 0$ mm, the retarding electrode is in contact with the suppressor electrode. At a position of $z = 3.81 - 0.64 = 3.17$ mm, the retarding electrode is in contact with the grounded electrode, since the thickness of the electrode is 0.64 mm. A schematic drawing of this change in position is shown in figure 20a. In figure 20b the value of k is plotted as a function of the position z.

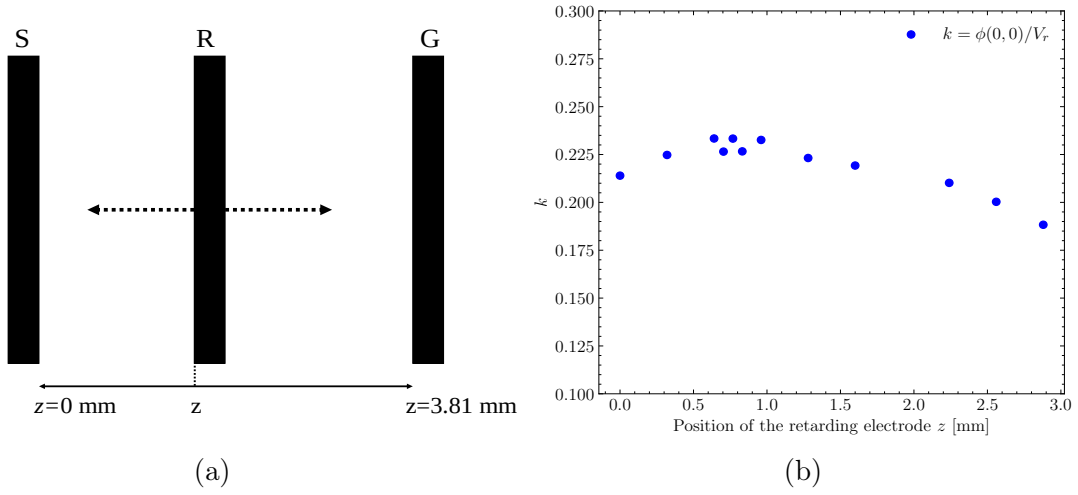

(a) (b)

Figure 20: A schematic drawing of how the position of the retarding electrode z is varied in between the suppressor and grounded electrode (figure 20a), and the value k plotted as a function of the position z (figure 20b).

The radius of the retarding electrode is set at $R = 4.765$ mm since this is the radius of the of electrode hole in the original design and the thickness of the retarding electrode at $d = 0.64$ mm. As was discussed in section 5.1.1 the value of k increases for a lower R, but if R is kept constant then the behaviour of k for varying z will stay the same. Figure 20b shows that varying the position of the retarding electrode barely influences the value of k. Furthermore, there seems to be a ragged peak between a position of 0.5 mm and 1 mm. This can be caused by the refinement of the SIMION model as the difference in z is on the scale of a grid unit. Changing z in the millimeter scale might be too insensitive to have a big effect on k, as this only changes in the order of 10^{-2}. Since increasing the thickness and decreasing the radius of the electrodes seem to be much more effective, changing the position of the retarding electrode will not be considered as an effective design change for a grid-less RFA.

5.2 Optimised SIMION Design

The results in the previous sections can be combined to create an RFA with a k value close to one. However, another thing to consider is the functionality of the suppressor electrode. The high potential field from the retarding electrode extends to the suppressor which causes the potential in the center of the negatively biased suppressor electrode to increase. Therefore, the suppressor loses its ability to inhibit secondary electrons to escape from the FC. This effect can be reduced by also reducing the radius of the suppressor electrode, increasing its length, or by adding an extra grounded electrode in between the retarding electrode and suppressor electrode. In figure 21a can be seen how adding an extra grounded electrode changes the potential in the RFA and in in figure 21b it can be seen how this lowers the potential in the suppressor electrode.

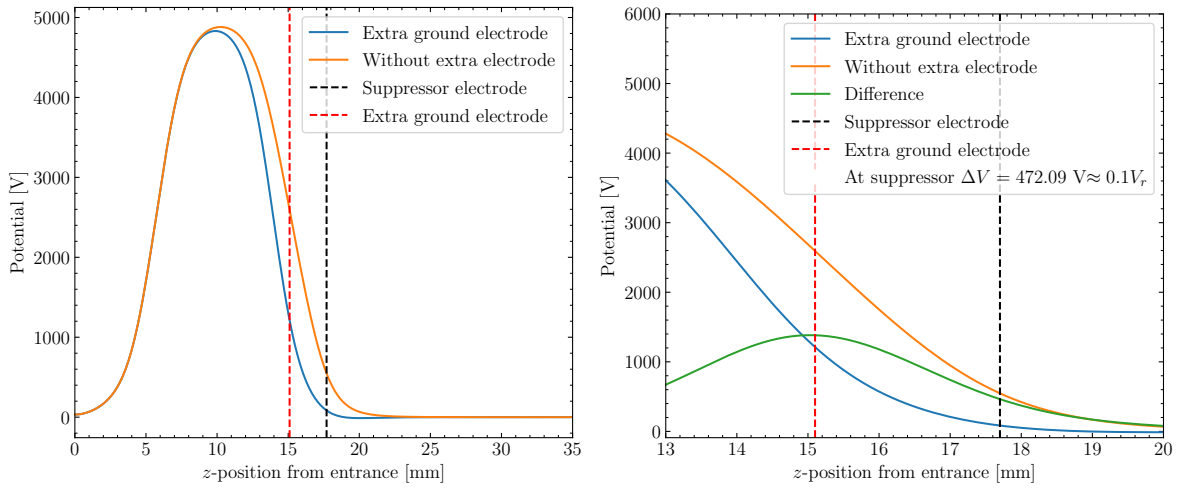

(a) (b)

Figure 21: The potential in a grid-less RFA with and without an extra grounded electrode for $V_r = 5000$ V and $V_s = -100$ V (figure 21a), and a close up of this potential around the suppressor electrode (figure 21b).

Adding the extra grounded plate seems to decrease the potential in the suppressor by $\Delta V = 472.09$ V $\approx 0.1 V_r$. Furthermore, the maximum difference in potential between these two scenarios is at the place where the extra grounded electrode is positioned. At lower retarding voltages, the effect of the retarding electrode increasing the potential in the suppressor electrode decreases, as the potential field of the retarding electrode does not extend as far to reach the suppressor electrode. This lower potential in the suppressor electrode will increase its k value k_s. As was shown before with the retarding electrode, decreasing the radius and increasing the thickness of the suppressor electrode will also increase k_s. The field from the retarding electrode can still extend to the suppressor electrode but its influence is less strong. To achieve a high value of k, the radius and thickness of the retarding electrode is chosen to be $R = 2.5$ mm and $d = 10 d_0 = 6.4$ mm, respectively. This same radius is given to the suppressor electrode and the extra ground electrode. The value of k for this RFA is determined to be $k \approx 0.96$. On the right in figure 18 it can be seen that the retarding electrode turns into

a very thick cylinder. It is redundant to have such a thick cylinder as only the inner radius has an influence on k. Therefore, the retarding electrode can also be reduced to a tube. This way, less material is used and the RFA will be less heavy. In figure 22a a possible SIMION design of a Grid-less RFA can be seen. And in figure 22b the potential landscape of this design can be seen for $V_r = 100$ V and $V_s = -100$ V. In figure 22a the retarding tube can be seen clearly.

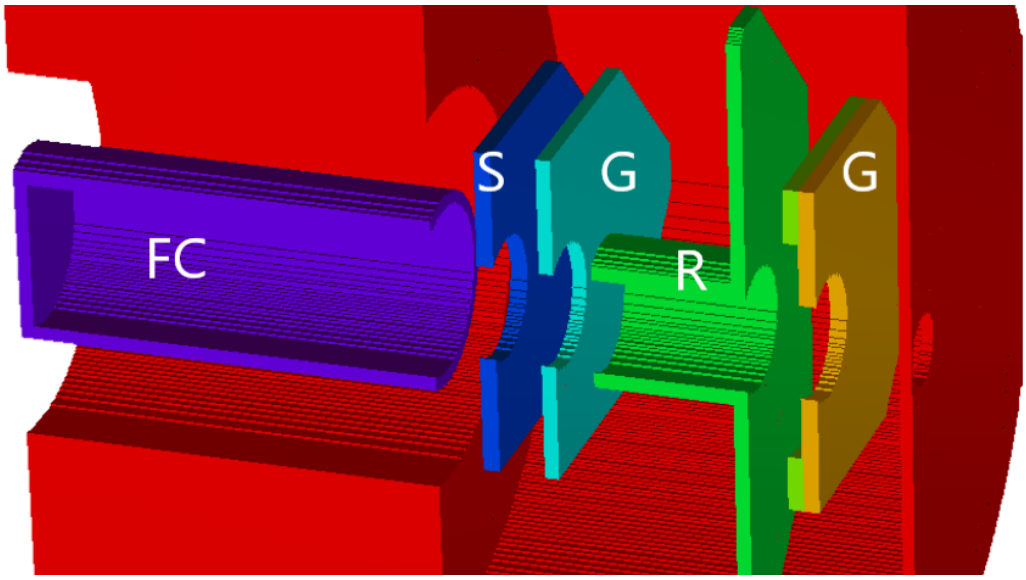

(a)

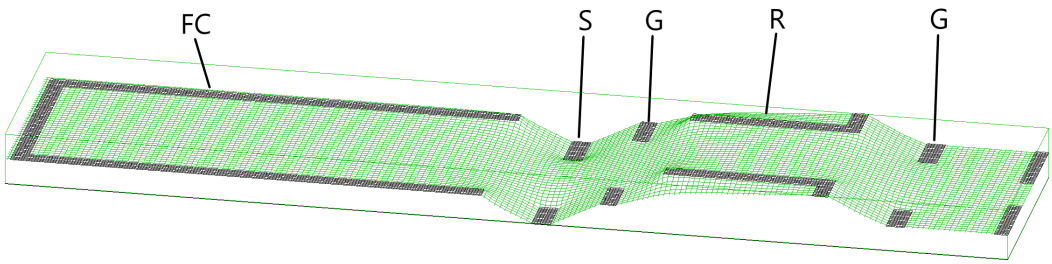

(b)

Figure 22: A possible SIMION design of a Grid-less RFA (figure 22a, and the potential landscape of the SIMION design with $V_r = 100$ V and $V_s = -100$ V (figure 22b). Note that the shapes of the electrodes and their orientation are taken from the original RFA design but these can also be circular.

Note that in this chapter the effects of geometric changes were discussed. The design shown in figure 22a is a possible design but this can be improved by tuning the thickness and radii of the electrodes in such a way that it complies with the real life requirements. With these adjustments to the design, the transmission of a monoenergetic multiply charged Sn beam with $q = 1+, 2+, 3+$ can be measured in SIMION as a show of concept. In this simulation the number of particles for each charge state is defined beforehand as $N^{3+} = 5000$, $N^{2+} = 3000$, and $N^{+} = 2000$ with $N_0 = 10000$. In reality these proportions are different but this way the charge states can be easily differentiated from each other. Figure 23 shows the transmission of this ion beam as a function of the retarding voltage. By making the necessary geometrical adjustments to the grid-less RFA to let $k \approx 1$, the lensing effects seen in a conventional RFA with grids have been eliminated since no grids are used.

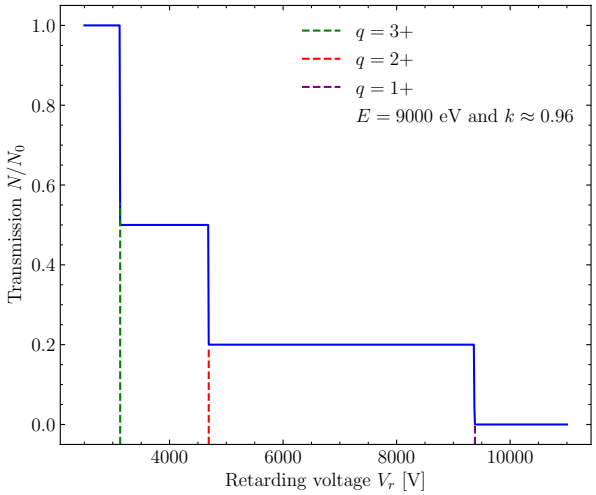

Figure 23: The transmission of a monoenergetic multiply charged Sn beam with $q = 1+, 2+, 3+$ and $E = 9000$ eV.

5.3 Final Grid-less RFA Design

The geometry shown in figure 22a is a proof of concept of a grid-less RFA. Based on the results from SIMION and the final geometry discussed in the section 5.2, a mechanical design was made by M. Salverda in a software package called Inventor. This design can be seen in figure 24a.

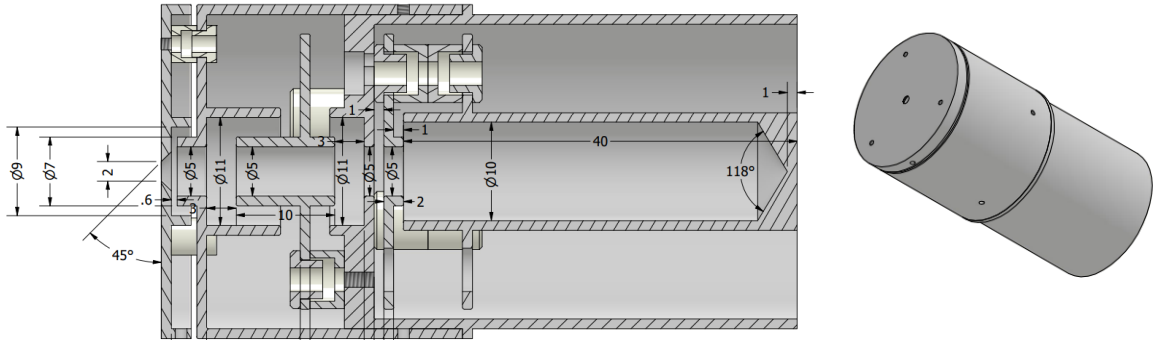

(a) (b)

Figure 24: Design for a grid-less RFA made in Inventor, with 24a being the inside of the RFA and 24b being the outside. This design was made by M. Salverda.

In figure 24a can be seen that all electrodes have a radius of $R = 2.5$ mm and the first ground electrode, the retarding electrode, the extra ground electrode, and the suppressor electrode have a thickness/length of $d = 3$ mm, $d = 10$ mm, $d = 1$ mm, and $d = 2$ mm, respectively. The first ground electrode also has an extra tube attached with a diameter of $d = 11$ mm that extends beyond the opening of the retarding electrode. The purpose of this extension is not to affect the transmission, but instead to prevent ions or electrons from colliding with the ceramics in between the electrodes. These ceramics are there to make sure the different electrodes are insulated from each other. If charged particles collide with the ceramics, the ceramic builds up charge and can generate an electric field which influences the transmission. With these extensions, it is impossible for the particles to interact with the ceramics. These kind preventive measures have also been applied to the diaphragm and the extra ground electrode. In the next chapter, different properties and functionalities of this design are tested.

6 SIMION Simulations of a Grid-less RFA

To discuss the functionality of the design seen in figure 24a, the CAD files of this design can be imported into SIMION and simulations can be done to test its functionality. In this chapter the potential field inside the grid-less RFA is illustrated, the functionality of the suppressor electrode is analysed, the transmission and energy resolution of the grid-less RFA will be discussed, and the ability of a grid-less RFA to detect energy distributions is shown.

6.1 The Potential in the Grid-less RFA

In figure 25 the equipotential lines in this RFA are shown for $V_r = 500$ V and $V_s = -100$ V. In this figure can be seen that the differently colored lines have different values of dV. What this means is that between each line of the same color, there is a potential difference of dV. This is done to illustrate how the potential changes in different areas. Within the red region in the retarding electrode, the total potential difference between the center of the retarding electrode $z = z_r$ and the edge of the red region is around 20 V. However, in the green region the total potential difference is around 300 V when moving along the z-axis. In figure 25 can also be seen that the potential around the suppressor electrode, displayed by the blue region, is negative and extends in to the FC to reflect any secondary electrons back into the FC.

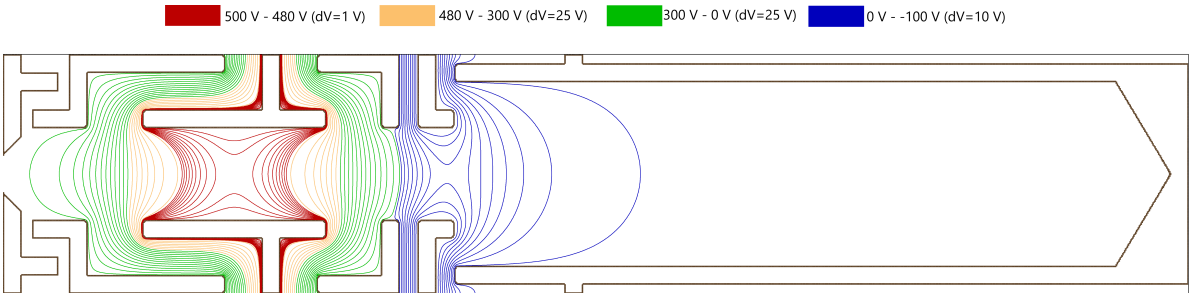

Figure 25: The equipotential lines of the RFA with $V_r = 500$ V and $V_s = -100$ V. In the legend above it can be seen that different values of dV are used for different colors. In the red region (500 V-480 V), the distance between two potential lines is 1 V. However, in the yellow and green regions $dV = 25$ V.

The change in potential along the z direction is way higher in the green region than in in the red region. Furthermore, in the red region the radial potential difference is also only a few Volts. Therefore in this regime,

$$\frac{\partial \phi(r, z_r)}{\partial r} \approx \frac{\partial \phi(0, z)}{\partial z} \approx 0.$$

This can be seen clearly when the potential gradient $\partial\phi/\partial z$ is plotted, as seen in figure 26. The radial potential and the radial potential gradient in the midplane of the retarding electrode can also be plotted which can be seen in figure 27a and 27b.

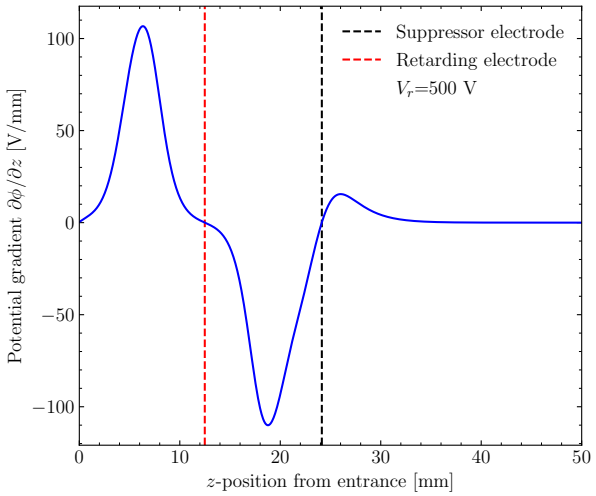

Figure 26: The potential gradient along the z-axis of the grid-less RFA. Here can be seen that the potential gradient is 0 at the position of the retarding electrode and the suppressor electrode.

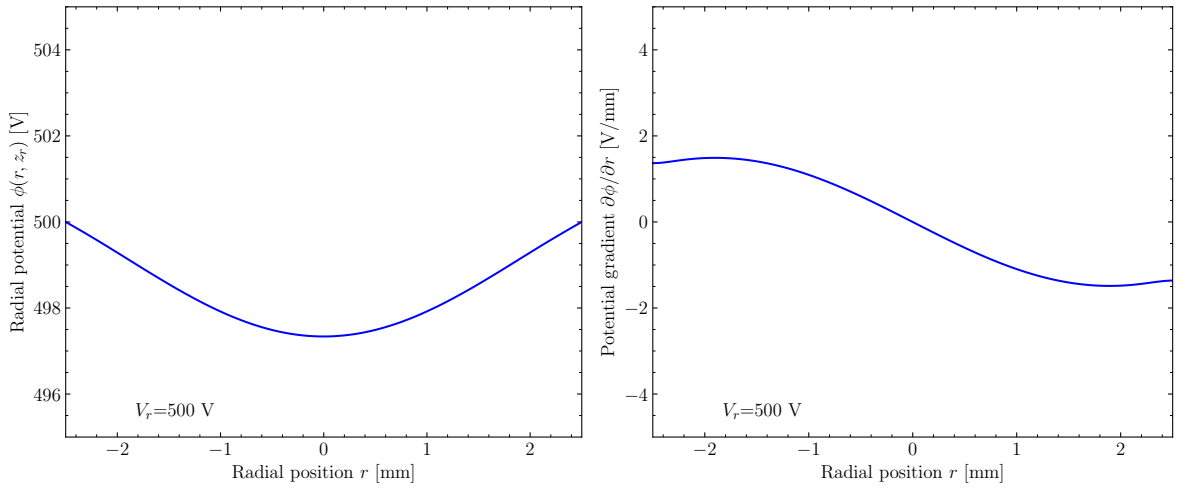

(a) (b)

Figure 27: The radial potential and potential gradient in the midplane of the retarding electrode of the grid-less RFA for $V_r = 500$ V.

From these figures it can be seen that the potential barely changes radially. Compared to a retarding voltage of $V_r = 500$ V, a change of a few volts can be neglected. Therefore,

$$\frac{\partial\phi(r, z_r)}{\partial r} \approx 0.$$

These properties imply that $k \to 1$ and thus,

$$\phi(0, 0) = kV_r \simeq V_r,$$

6.2 The Suppressor Electrode

The suppressor electrode of the grid-less RFA makes sure that secondary electrons generated in the FC do not escape from the FC. The design of the FC has as rule of thumb that $L/d > 4$, where L is the length of the FC and d is the diameter of the FC such that, even without a suppressor electrode, secondary electrons will mostly collide inside the FC itself. The kinetic energy of secondary electrons is generally between 0-25 eV [9], so the suppressor electrode needs to be able to reflect electrons within this energy range back into the FC. Since the suppressor electrode is usually set at around $V_s = -100$ V but the retarding electrode can get to around $V_r = 10000$ V, it is interesting to see how the retarding electrode affects the potential within the suppressor electrode. In figure 28 the potential within the suppressor electrode is plotted as a function of the z position from the entrance of the grid-less RFA where $V_s = -100$ V.

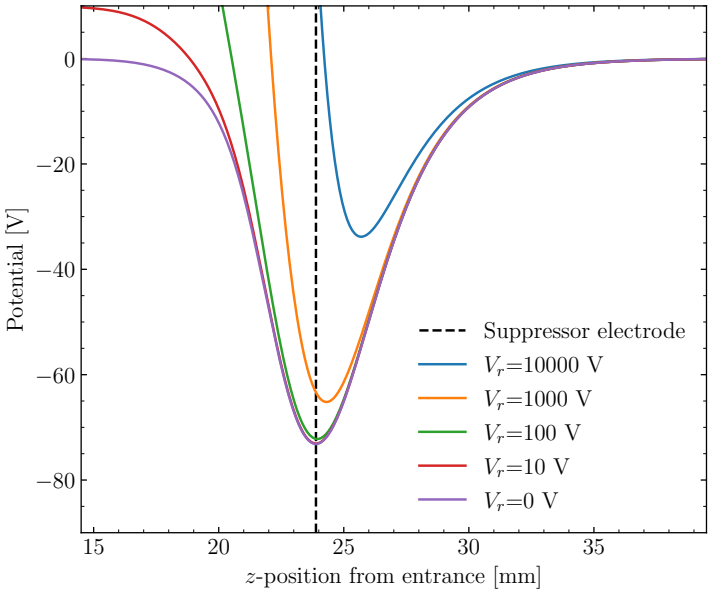

Figure 28: The potential in the grid-less RFA along the z-axis around the suppressor electrode for various retarding voltages with $V_s = -100$ V.

In figure 28 can be seen that with an increasing V_r the minimum potential in the suppressor also increases. Therefore, the k value of the suppressor k_s will decrease with a higher V_r. At $V_r = 0$ V and $V_r = 10$ V the potential is around $V = -70$ V which gives $k_s \approx -70/-100 = 0.7$. However, at $V_r = 10000$ V the potential can get to around $V = -30$ V which gives $k_s \approx 0.3$. This means that the suppressor voltage should be chosen such that even at high retarding voltages the suppressor electrode can still reflect secondary electrons back into the FC.

To see how the retarding voltage affects the functionality of the suppressor electrode, SIMION simulations were done where electrons were emitted from the FC as shown in figure 29.

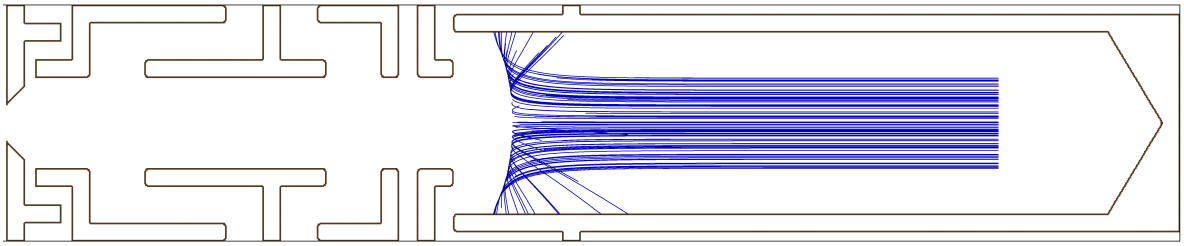

Figure 29: SIMION simulation of secondary electrons being emitted from the FC and being fully reflected back into the FC.

In reality, this is not how secondary electrons are emitted from the FC. They are emitted from the surface of the FC and the direction of the electrons is more of a distribution of angles. However, since the suppressor just needs to be able to reflect electrons back into the FC, the direction of all the electrons are chosen to be towards the suppressor electrode. In figure 30a the results are shown for a simulation where the kinetic energy of the electrons is set to $E = 5$ eV and the suppressor voltage is varied from 0 to -100 V for various retarding voltages. From this it can be seen that the suppressor voltage at which all the secondary electrons are fully reflected back into the FC, becomes lower for higher retarding voltages. However, electrons with a kinetic energy of $E = 5$ eV are fully reflected at $V_s \approx -40$ V even at $V_r = 10000$ V. So setting V_s to -100 V makes sure it is impossible for electrons with $E < 5$ eV to escape the FC.

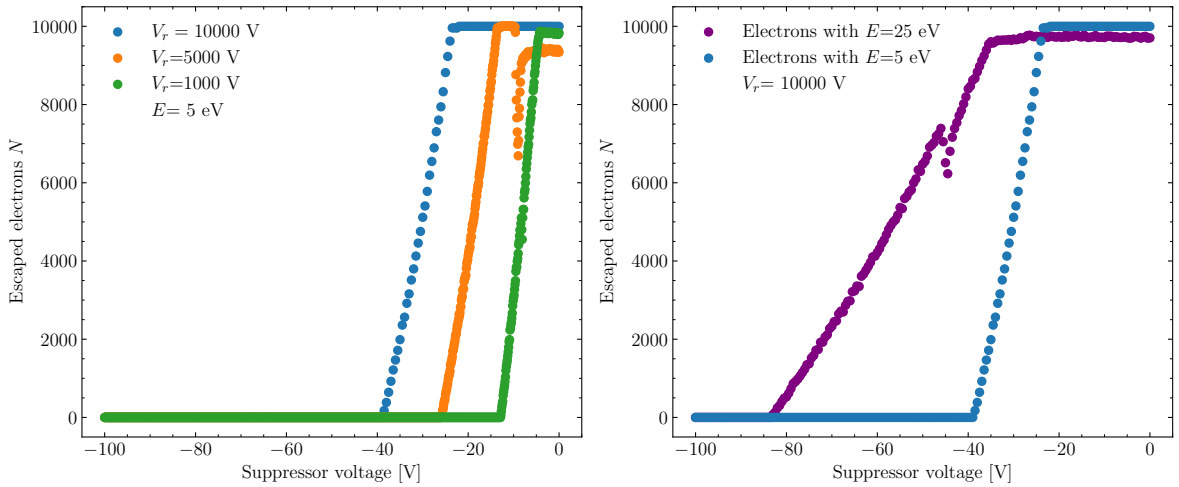

(a) (b)

Figure 30: The amount of electrons with $E = 5$ eV that escape the FC for varying V_s at different V_r (30a) and a comparison between electrons of $E = 5$ eV and $E = 25$ eV at $V_r = 10000$ eV (30b).

To see how the suppressor electrode functions for secondary electrons with higher kinetic energies, simulations were done for electrons with $E = 5$ eV and $E = 25$ eV where the suppressor voltage is varied from 0 to -100 V for a constant retarding voltage of $V_r = 10000$ V. The results of this simulation can be seen in figure 30b. In this figure it is shown that even for kinetic energies of $E = 25$ eV, the secondary electrons are still fully reflected at a suppressor voltage of around $V_s \approx -80$ V. Therefore, setting the suppressor voltage at $V_s = -100$ V can fully reflect secondary electrons with an energy distribution in between 0 - 25 eV even at a retarding voltage as high as $V_r = 10000$ V.

In figure 30a for $V_r = 5000$ V at $V_s \approx -10$ V, the number of escaped electrons quickly decreases before it increases back to its maximum and then decreases to zero at a lower V_s. In figure 30b for $E = 25$ eV, this same effect can be seen at $V_s \approx -50$ V. The reason for this effect is unknown and further simulations need to be done to gain further understanding of why this happens. However, this does not influence the ability of the suppressor electrode to reflect electrons back into the FC.

6.3 Transmission and Energy Resolution of a Grid-less RFA

The purpose of an RFA at ZERNIKELEIF is to distinguish particles of different charge states. In SIMION, simulations can be run for ion beams with different charge states or energies. This ion beam will be analysed by the grid-less RFA. In figure 31a, the trajectories of the ions can be seen where their trajectory is altered due to the potential set on the retarding electrode but are still fully transmitted. Furthermore, in figure 31b a fully reflected ion beam can be seen.

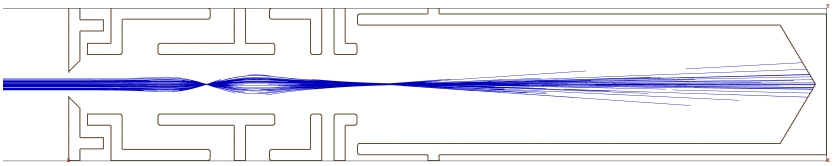

(a)

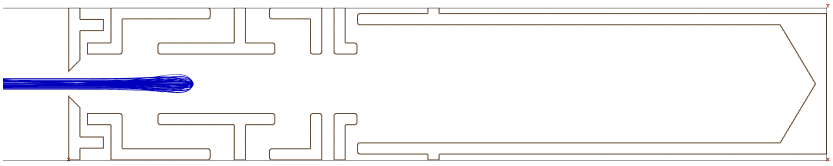

(b)

Figure 31: Ion trajectories in SIMION for an ion beam where the trajectories are altered due to the retarding electrode (31a) and a fully reflected ion beam (31b).

Just like was done in figure 23, a SIMION simulation was done where the abundance of charge states is measured for a multiply charged, monoenergetic Sn beam with $q = 1+, 2+, 3+$ and $E = 9000$ eV. The transmission of this simulation can be seen in figure 32.

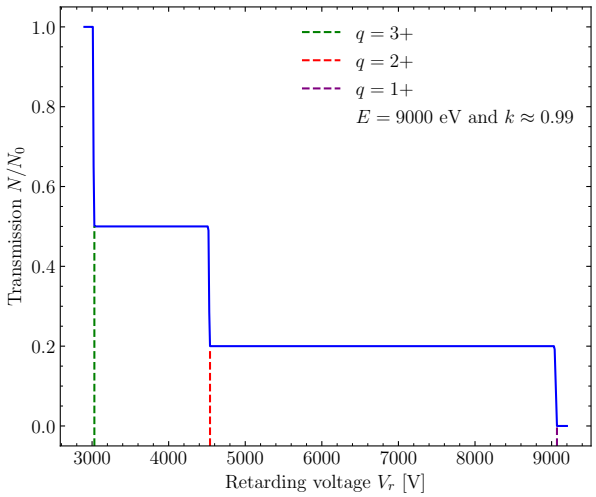

Figure 32: The transmission of a multiply charged, monoenergetic Sn beam with $q = 1+, 2+, 3+$ and an energy of $E = 9000$ eV.

Figure 32 looks almost identical as the transmission in figure 23, but the value of k is $k \approx 0.99$ instead of $k \approx 0.96$. This value of k is in line with the statement made in section 6.1 that $k \to 1$. Up until now, only monoenergetic ion beams of $E = 9000$ V have been investigated. To see if the grid-less also works for lower energies, the simulation done for figure 32 has also been done for kinetic energies of $E = 100$ eV and $E = 10$ eV. The results of these simulations can be seen in figure 33a and 33b.

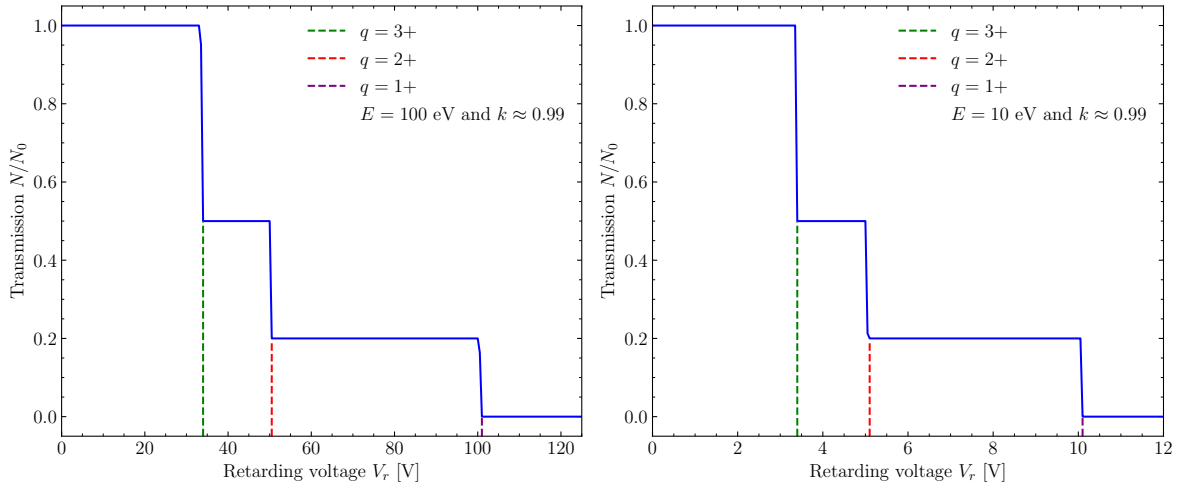

(a) (b)

Figure 33: The transmission for Sn beams with $q = 1+, 2+, 3+$ and kinetic energies of $E = 100$ eV (33a) and $E = 10$ eV (33b).

In an RFA with grids, lensing effects occur around the voltage at which the ions almost get blocked (see figure 4). To see how a grid-less RFA affects the transmission at this point, a close up around such voltage is simulated for a monoenergetic Sn beam with $E = 10$ eV and $q = 1+$. For this energy and charge state, the retardation voltage will be at $V_r = 10$ V, and small voltage increments are used of $dV = 0.001$ V but with a total amount of ions per increment of $N = 1000$. The result of this simulation can be seen in figure 34.

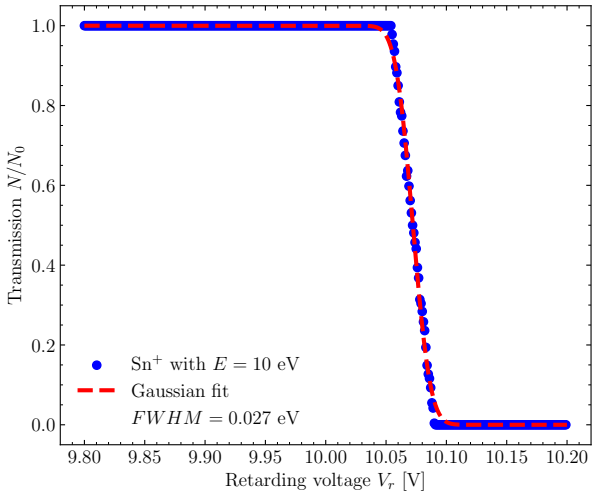

Figure 34: The transmission around the point of full retardation of an Sn^+ beam with $E = 10$ eV with a Gauss error function fit with a $FWHM = 0.027$ eV.

In the figure above, a Gauss error function was fitted to the steeply declining transmission curve. From this error function a Gaussian can be retrieved with a Full Width Half Maximum of $FWHM = 0.027$ eV. With $FWHM = 0.027$ eV the energy resolution for the grid-less RFA is determined to be $FWHM/E = 0.027/10 = 0.27\%$. However, the actual energy resolution might in reality be lower as the time of flight increases because of the longer drift zone [10]. Further simulations and experiments need to be done to determine this energy resolution.

In figure 34 it can clearly be seen that there are no lensing effects occurring. Therefore, by removing the grids and adjusting the design of an RFA, lensing effects that a conventional RFA does have, can be eliminated while maintaining an accurate energy resolution.

6.4 Energy Distribution Detection

At ZERNIKELEIF monoenergetic ion beams are used to measure the charge exchange between Sn ions and H_2 gas. But RFA's can also be used to measure the energy distribution of a beam of charged particles [4]. To see if a grid-less RFA is a suitable device to measure such distributions, SIMION simulations were done with an ion beam with $q = 1+$ and a Gaussian energy distribution with a mean of $\mu = 5000$ eV and $FWHM = 800$ eV. These values were chosen as a show of concept, and are only used to showcase that both these values can be retrieved using a grid-less RFA. In reality, the $FWHM$ of these energy distributions is a lot smaller. The results of this simulation can be seen in figure 35a and 35b.

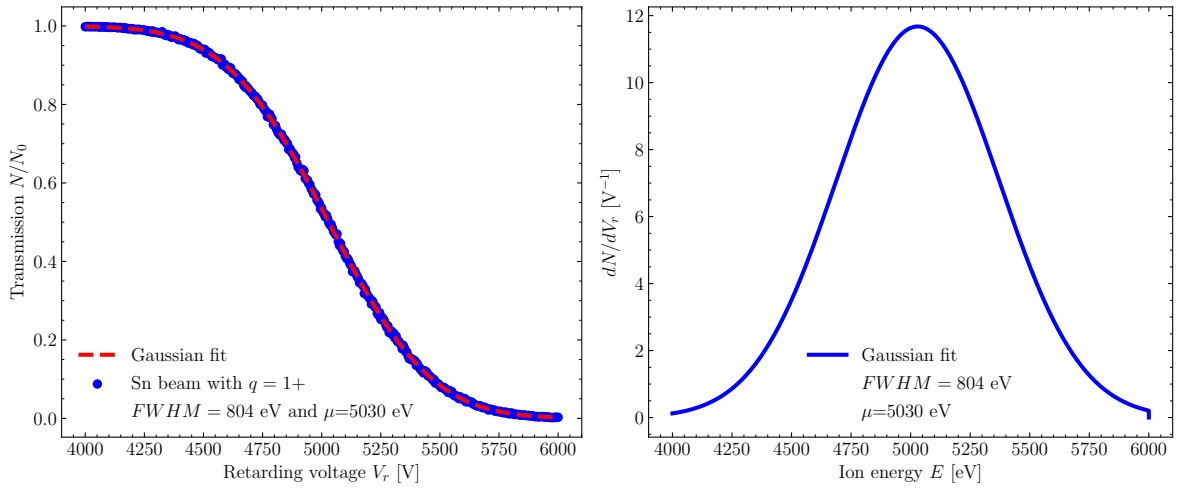

(a) (b)

Figure 35: The transmission fitted by a Gauss error function at each retarding voltage of an ion beam with a Gaussian energy distribution with a mean of $\mu = 5000$ eV and $FWHM = 800$ eV (35a), and the resulting Gaussian when the errorfunction is differentiated with respect to V_r (35b).

In figures 35a and 35b it can be seen that the energy distribution of a singly charged ion beam can be measured with a fairly high accuracy. The reason dN/dV_r is used to determine the energy distribution, is because it describes how many particles of a certain energy and charge get fully reflected at a specific retarding voltage. This means that these particles have a specific energy to charge ratio that is equal to the retarding voltage. Such that the energy of these ions is $E = qV_r$.

Even though the mean and $FWHM$ can be retrieved fairly accurately, the value of μ still differs by 30 eV. However, this is only a small discrepency of 0.6% of the mean μ and is therefore insignificant. The same holds for the $FWHM$ where there is only a 0.5% difference between the input and output value. The same simulation was done with μ=50 eV and a $FWHM$=8 eV and the results can be seen in figure 36a and 36b, where the differences in the mean and $FWHM$ are also 0.6% and 0.5%, respectively.

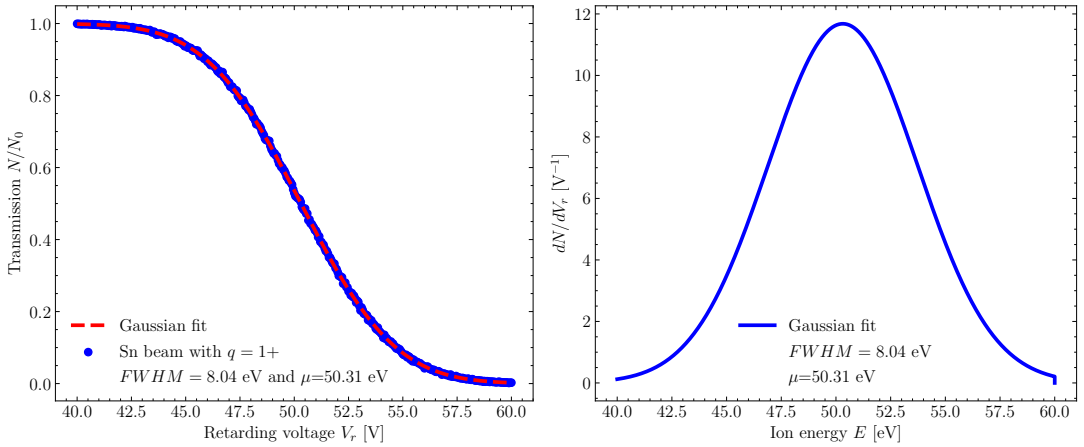

(a) (b)

Figure 36: The same simulations done as figures 35a and 35b, but then with input values of μ=50 eV and $FWHM$=8 eV.

This same method can be used for a multiply charged ion beam with a Gaussian energy distribution. In the simulation, a mean energy of $\mu = 6000$ eV was used with $FWHM = 800$ eV. For this transmission, three different error functions need to be fitted for each charge state. The transmission and the resulting error functions can be seen in figure 37a and their respective Gaussian fit for their energy distribution can be seen in figure 37b. The mean μ and the $FWHM$ of the different charge states can be

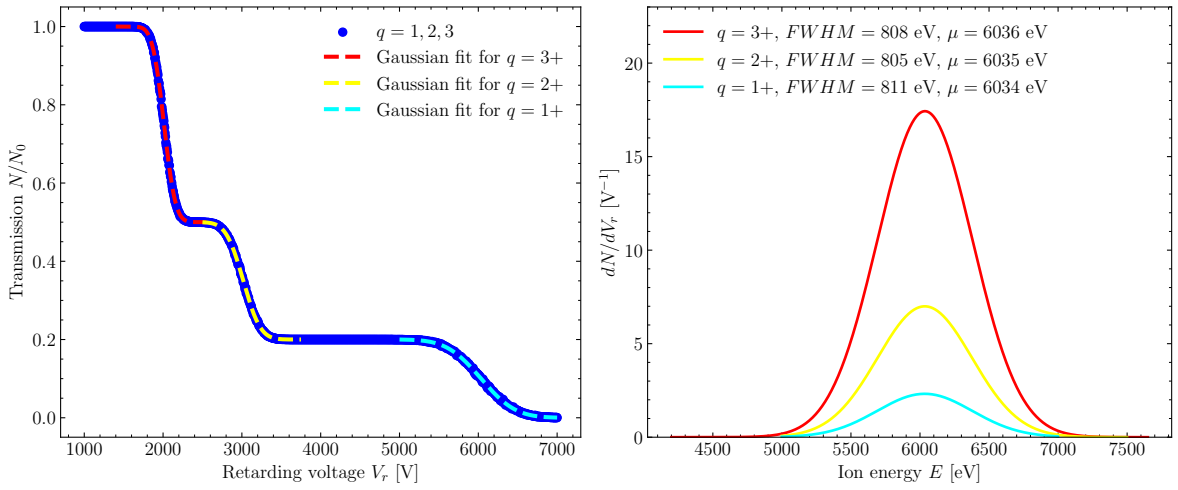

(a) (b)

Figure 37: The transmission and a Gaussian fit of the change in particles at each retarding voltage of a multiply charged ion beam and a Gaussian energy distribution with a mean of $\mu = 6000$ eV and $FWHM = 800$ eV.

seen in figure 37b, where these values also differ only sleightly from their input values. From these figures can be seen that the energy distributions of the different charge states can be measured with a fairly good accuracy with a grid-less RFA.

7 Conclusion

In order to measure the charge exchange between Sn ions and H_2 gas, an RFA is used to distinguish different charge states from each other. However, current generation RFA's make use of grids which causes the transmission to become dependent on the retarding voltage V_r. When the retarding voltage approaches the retardation voltage, the incoming ion beam gets focused on the suppressor electrode which causes the FC current to decrease before it increases again since the ions are not focused on the suppressor grid anymore. Furthermore, due to ion collisions with such grids, secondary electrons can be emitted. These secondary electrons cannot be prevented to enter the FC when they are generated from the suppressor grid.

In this thesis, a proposal for a grid-less RFA is made. The potential field within an electrode and its dependence on the geometrical properties of the electrode are described in detail. The model of an electrode with a hole described by Sakai is used as a basis on how the geometry of an electrode influences the potential field within the electrode. By increasing the thickness and decreasing the radius of the retarding electrode, the ratio k between the potential at the center of the electrode $\phi(0,0)$ and the retarding voltage V_r approaches 1. From the design process that was described in chapter 5, a new mechanical design was made by Mart Salverda in a software package called Inventor.

In chapter 6, the properties of the new grid-less RFA design were discussed. The potential gradient in the z and r direction seems to approach 0 at the center of the retarding electrode which implies that $k \to 1$ such that $\phi(0,0) \simeq V_r$. Furthermore, it was shown that an increasing retarding voltage also increases the potential at the center of the suppressor electrode. This causes the value of k_s to decrease from $k_s \approx 0.7$ to $k_s \approx 0.3$, which means that the effectiveness of the suppressor electrode decreases. To test how this changes the effectiveness of the suppressor electrode, SIMION simulations were done for secondary electrons emitted from the FC where V_s was varied from 0 to -100 V for various retarding voltages. These simulations show that even at retarding voltages as high as $V_r = 10000$ V, secondary electrons with $E = 5$ eV and $E = 25$ eV will be reflected back into the FC around $V_s = -40$ V and $V_s = -80$ V, respectively. Therefore, setting the suppressor voltage at $V_s = -100$ V will ensure that the suppressor electrode works as intended for electrons in the $E < 25$ eV range.

In section 6.3, the transmission for multiply charged Sn ion beams for various energies were simulated as a show of concept on how different charge states can be distinguished from each other. The value of k was also determined to be $k \approx 0.99$ which confirms the statement made in section 6.1 that $k \to 1$ for this design. To see how the transmission behaves around the retardation voltage of an ion beam, a simulation was done with a monoenergetic ion beam of $E = 10$ eV with $q = 1+$ for retarding voltages between 9.8 V and 10.2 V with $dV = 0.001$. By fitting a Gauss error function and calculating its $FWHM$, the energy resolution of this grid-less RFA was determined to be 0.27%. However, the actual energy resolution might differ from this value as the time of flight increases due to the longer drift zone. Further simulations need to be done to determine

how this influences the energy resolution.

Besides measuring different charge states, an RFA can also be used to measure the energy distribution of a beam of charged particles. It was shown that a grid-less RFA is also able to detect the mean and Full Width Half Maximum of energy distributions with an accuracy of 0.6% and 0.5%, respectively. Furthermore, even the energy distributions of different charge states in a multiply charged ion beam can be determined.

With conventional RFA's, one of the main problems is the lensing effects caused by the grids, and the grid dependent transmission. By using a grid-less RFA, no lensing effects were observed in the simulations while still maintaining a high energy resolution. Since no grids are used this also solves the problem of a grid dependent transmission.

As this thesis only includes simulations of a grid-less RFA, further experimental measurements need to be performed to confirm the findings of these simulations.

8 Acknowledgements

Ronnie, thank you for giving me a project that I can work on independently and allowing me to take my time during a busy year in my life. Even though I was mostly in the office instead of the laboratory, I am happy I got to work on a project that has tangible results. Also thanks to Luc Assink for being my daily supervisior and guiding me through this project. Thanks to Robbert Jullius for helping me when I had questions about SIMION. Furthermore, thanks to Emiel de Wit and Klaas Bijlsma for the interesting conversations about the principles of RFA's. Also thanks to Thomas for taking the time to read and grade my thesis. And lastly, many thanks to Mart Salverda for making the actual design of the grid-less RFA based on my simulations and for assembling the actual grid-less RFA.

References

[1] G. O'Sullivan, D. Kilbane, and R. D'Arcy, "Recent progress in source development for extreme UV lithography," *Journal of Modern Optics*, vol. 59, no. 10, 2012.

[2] O. O. Versolato, "Physics of laser-driven tin plasma sources of EUV radiation for nanolithography," *Plasma Sources Science and Technology*, vol. 28, no. 8, 2019.

[3] L. Assink, "The potential dependent transmission of a four-gridded retarding field analyzer," University of Groningen, Tech. Rep., 2022.

[4] T. Van De Ven, C. De Meijere, R. Van Der Horst, M Van Kampen, V. Banine, and J Beckers, "Analysis of retarding field energy analyzer transmission by simulation of ion trajectories," *Review of Scientific Instruments*, vol. 89, no. 4, 2018.

[5] S. Rai, K. Bijlsma, I Rabadán, *et al.*, "Charge exchange in collisions of 1–100-keV Sn^{3+} ions with H_2 and D_2," *Physical Review A*, vol. 106, 2022.

[6] Y. Sakai and I. Katsumata, "An energy resolution formula of a three plane grids retarding field energy analyzer," *Japanese Journal of Applied Physics*, vol. 24, 1985.

[7] J. Hwang, K.-I. Kim, T. Ogawa, B. Cho, D.-H. Kim, and I.-Y. Park, "Study and design of a lens-type retarding field energy analyzer without a grid electrode," *Ultramicroscopy*, vol. 209, 2020.

[8] S. Rai, "Ionic interactions around EUV generating tin plasma," Ph.D. dissertation, University of Groningen, 2023.

[9] M. J. Deuzeman, "Generation and interactions of energetic tin ions," Ph.D. dissertation, University of Groningen, 2019.

[10] L. Assink, "Design analyses for a new experimental rig to study the energy loss of Sn ions in H_2 gas," M.S. thesis, University of Groningen, 2022.